A robust maximum power point tracking from wind turbines using fractional order PI controller

Abdelfatah El ouadiki[1*], *Mohammed Taoussi*[1,2], and *Mohammed Es-salmi* [1]

[1]Industrial Technologies and Services Laboratory, Higher School of Technology, Sidi Mohamed Ben Abdellah University, Morocco
[2]Spectrometry of Materials and Archaeomaterials Laboratory, Higher School of Technology, Moulay Ismail university, Meknes, Morocco

Abstract. Wind Advanced and adaptive control methodologies are necessary to ensure optimal operation of wind power systems under variable climatic conditions. In this article, a new MPPT technique using a fractional-order proportional-integral PI^{λ} controller is proposed for for doubly-fed induction generator (DFIG)-based wind turbines and validated using a real wind profile from Dakhla. The controller parameters are optimized through MATLAB scripts using a frequency-domain tuning approach that ensures system stability and practical implementation via a low-order rational approximation. Simulation results demonstrate that the proposed PI^{λ} controller significantly accelerates convergence to the maximum power point, reduces response time by up to 92%, and enhances precision, stability, and robustness compared to the conventional PI controller. Moreover, the computational load associated with the fractional term remains compatible with real-time implementation (dSPACE/FPGA), paving the way for practical integration into modern wind energy systems.

1 Introduction

The current transformation of the energy sector favors the increased integration of renewable energies into production processes. In this context, wind power is crucial due to its availability, low carbon emissions and competitive production costs. Renewable energy sources, such as wind, are preferred because of their beneficial ecological impact compared with that of traditional fossil fuels. However, as wind energy production is largely influenced by geographical and meteorological factors, it is necessary to set up a system that maximizes production by integrating these elements. [1,2]. Depending on the intensity of the wind, a wind turbine converts the kinetic energy of the wind into mechanical energy, before converting it into electricity via a generator. Today, many wind turbines use doubly-fed induction generators (DFIG). These conversion systems, based on DFIG technology, offer significant advantages for variable-speed applications, thanks to their high efficiency, ability to control reactive power and suitability for compact power converters [3,4]. The general structure of the variable-speed wind turbine system based on a DFIG is represented by Fig.1.

* Corresponding author: abdelfatah.elouadiki@usmba.ac.ma

© The Authors, published by EDP Sciences. This is an open access article distributed under the terms of the Creative Commons Attribution License 4.0 (https://creativecommons.org/licenses/by/4.0/).

However, the amount of energy generated by wind turbines fluctuates non-linearly according to sudden and often unexpected variations in wind speed. This uncertainty complicates the efficient use of energy. The use of an MPPT controller is therefore essential to adapt the generator speed in real time and improve the evaluation of the outgoing power, in order to ensure optimal energy recovery, whatever the wind conditions.

The aim of the MPPT management algorithm is to locate and maintain the optimum power point (MPP) continuously, regardless of wind variations. With this in mind, numerous control techniques have been developed over the years to guarantee this essential functionality : ranging from optimal speed ratio tuning [5] to more sophisticated methods, such as the non-linear complex integral proportional (PCI) controller, fuzzy control systems [6,7], artificial neural networks (ANNs)[8], robust control strategies [9], wind speed-based Direct Torque Control (DTC) [10], as well as wind speed-adapted MPPT algorithms [11].

Among existing methods, the proportional-integral (PI) controller stands out for its ease of use, its widespread adoption in industry, and its effectiveness in managing power in systems with little disturbance. However, its effectiveness can diminish in complicated dynamic environments or in the presence of system uncertainties.

In order to overcome these constraints, fractional order control has recently been proposed as an interesting solution. The fractional-order PI controller PI^{λ}, which incorporates a notion of non-integer order, makes it possible to fine-tune the dynamic behavior of the system, offering an improved balance between stability, precision and robustness.

In this study, a novel MPPT strategy based on a fractional-order PI controller is presented and applied to a real wind profile recorded in Dakhla. The fractional parameters are optimized using MATLAB scripts that employ a multi-objective cost function that reduces steady-state error and control effort while respecting frequency domain constraints. The adjustment order, which clarifies a transition frequency and a target phase, also ensures system stability and practical feasibility by rationally reducing the number of operators. The simulation results, including windy conditions, showed significant improvements: the reaction time, which was previously 0.025 s, was reduced to 0.002 s; the steady-state error decreased from 0.45% to 0.15%; and the overshoot also decreased by 0.130%. Compared to established approaches such as OTC and Backstepping, compared to well-known methods such as OTC and Backstepping, the newly designed controller offers faster MPPT convergence, higher tracking accuracy, and an excellent balance between performance robustness and computational cost These properties make future real-time implementation on dSPACE or FPGA platforms possible and appropriate.

Comparison of the experimental data reveals that the new fractional-order PI controller we have designed is significantly better than the traditional PI controller in several respects - not only is the control accuracy higher, but the ability to track the target value is better, and overall performance is also significantly improved. This study is divided into several clear stages. Following this introduction, Section 2 focuses on the mathematical modelling of the wind turbine, with particular emphasis on its fundamental mechanical components. Section 3 then outlines the innovative control strategy we propose. Section 4 then presents and interprets in depth the results of the numerical simulations obtained. Section 5 provides a comparison of the control strategies implemented with other commonly used MPPT methods. Finally, Section 6 closes the paper by summarising the major findings and opening up future perspectives.

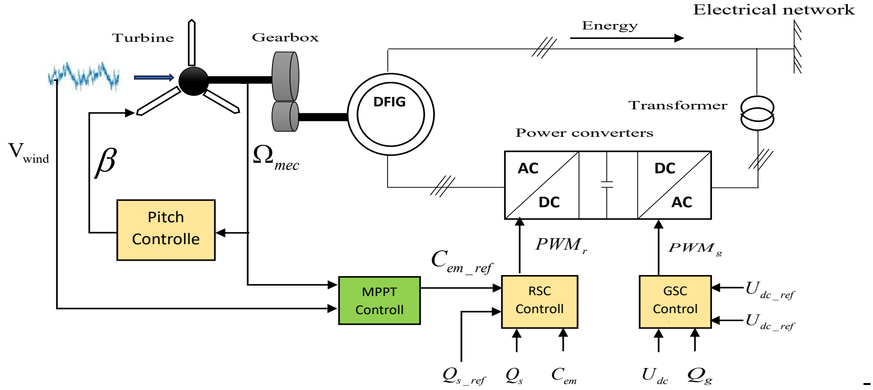

Fig.1. Structural illustration of a DFIG variable-speed wind generator

2 Modeling of wind energy conversion system

The mechanical power and torque are described as follows [12].

$$P_t = C_p(\lambda,\beta)\cdot\frac{\rho S V^3}{2} \tag{1}$$

$$P_t^{opt} = C_p^{\max}(\lambda_{opt},\beta_{opt})\cdot\frac{\rho S V^3}{2} \tag{2}$$

$$C_t = \frac{P_t}{\Omega_t} \tag{3}$$

$$C_p(\lambda,\beta) = 0.0068\lambda + \frac{1}{2}\left(\frac{116}{\lambda_i} - \frac{2}{5}\beta - 5\right)\cdot\exp\left(\frac{-21}{\lambda_i}\right) \tag{4}$$

$$\frac{1}{\lambda_i} = -\frac{0.035}{\beta^3+1} + \frac{1}{\lambda + 0.08\beta} \tag{5}$$

$$\lambda = \frac{R_t\Omega_t}{V} \tag{6}$$

The mechanical power P_t of a wind turbine depends on several parameters: the wind speed V ,blade radius R , air density ρ, and power coefficient (see Fig. 2) demonstrates how the power coefficient has changed over time in relation to various speeds (λ) at each blade pitch angle (β) [13]. It shows that for each blade pitch angle β , there exists an optimal tip-speed ratio λ that maximizes the power coefficient C_p . Additionally, C_{pmax} of 0.48 occurs at $\beta = 0$ degrees, with a corresponding constant optimal ($\lambda_{opt} = 8.16$).

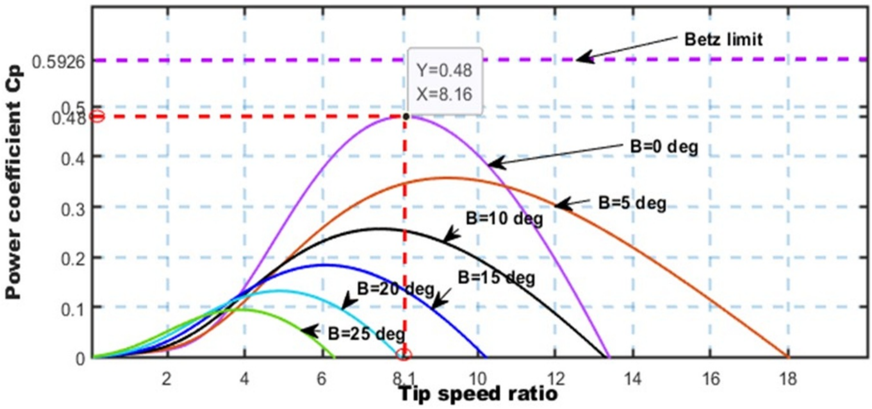

Fig.2. Power coefficients $C_p(\lambda,\beta)$.

The power of the wind turbine P_t , governed by equation (9), is highly sensitive to even the slightest fluctuations in wind speed. A gearbox is therefore essential to adapt the low speed of the rotor shaft to the high speed required by the generator. To simplify the model, we consider an ideal gearbox, which neglects elasticity, friction, and, consequently, the associated energy losses. The mathematical representation of this ideal gearbox is given by:

$$\Omega_t = \frac{\Omega_g}{G} \tag{7}$$

Ω_t and Ω_g represent the angular velocity of the turbine and that of the generator, respectively, while G is the conversion factor.

3 Mppt with speed regulation

The control strategies revolve around generator electromagnetic torque adjustment C_{em} to drive mechanical velocity Ω towards a referential value. This reference speed maximizes the wind turbine's captured power, as demonstrated in (6) Consequently, precise generator speed control is crucial. At any Specified operating point (constant windspeed), the maximum power output from the wind system is achieved when the coefficient of power C_p reaches its peak value. This peak typically occurs when the tip-speed ratio λ reaches its optimal value λ_{opt} .The corresponding optimal generator speed command for maximum wind power extraction is determined by:

$$\Omega_g^* = \frac{G \times V}{R}\lambda_{opt} \tag{8}$$

Figure 3 shows the structure of the wind turbine system, including the aerodynamic, mechanical, and control models. The aerodynamic model determines C_t and C_p according to λ and β, while the mechanical model links Ω_t and Ω_g via G , considering the total inertia J and the viscous friction coefficient F_v . The electromagnetic torque C_{em} , adjusted by the PI or PI^{λ} controller, controls the generator speed and ensures maximum power extraction.

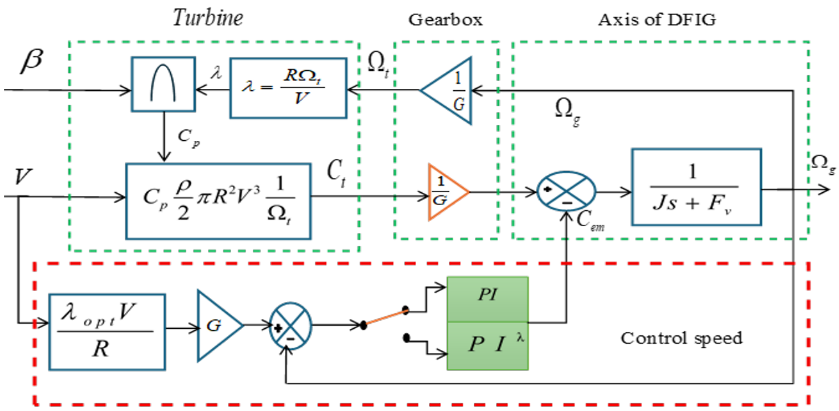

Fig.3. MPPT strategy with speed control.

3.1 Fractional-Order Control for MPPT in Wind Turbine Systems

Fractional calculus extends the traditional ideas of integration and derivation to non-integer orders, denoted by. In this context, the limits of the operation are symbolized by a and t, while characterizes the order of the operator. This fractional operator can be formulated as follows [14]:

$$aD_t^{-\lambda} = \begin{cases} \frac{d^\lambda}{dt^\lambda} & si\ \lambda > 0 \\ 1 \quad si & \lambda = 0 \\ \int_a^t (d\tau)^\lambda & si\ \lambda < 0 \end{cases} \tag{9}$$

The fractional operator according to Riemann-Liouville is defined as follows:

$$a\,D_t^{-\lambda} f(t) = \frac{1}{\Gamma(\lambda)} \int_a^t \left(t-\tau\right)^{\lambda-1} f(\tau)d\tau \tag{10}$$

$$a\,D_t^{-\lambda} f(t) = \frac{1}{\Gamma(n-\lambda)} \frac{d^n}{dt^n}\left[\int_a^t \frac{f(\tau)}{\left(t-\tau\right)^{\lambda-n+1}} d\tau\right] \tag{11}$$

With

$$\Gamma(x) = \int_0^\infty y^{x-1} e^{-y} dy \tag{12}$$

In this study, the fractional order index is assumed to satisfy the constraint. With the notation introduced below, the time domain differential equation of the fractional order controller can be expressed as:

$$u(t) = k_p\left(e(t) + k_i D_t^{-\lambda} \times e(t)\right) \tag{13}$$

In the expression, represents the integration constant introduced during the calculation process. The term denotes as the error between setpoint and system output. The parameter corresponds to the proportional gain applied to this error, while defines the fractional order of the integration operator. The latter allows more flexible adjustment of system dynamics than conventional integer-order controllers.

3.1.1 MPPT Algorithm based on PI-Controller

Let's take λ=1. We replace in formula 10:

We find: $D_t^{-1} f(t) = \frac{1}{\Gamma(1)} \int_0^t \left(t-\tau\right)^0 f(\tau) d\tau$

But we have:

$\Gamma(1) = 1$ and $\left(t-\tau\right)^0 = 1$

The PI controller time equation is given by:

$u(t) = k_p \left(e(t) + k_i D_t^{-1} \times e(t) \right)$

Substituted $D_t^{-1} \times e(t)$ by the classical integral:

$u(t) = k_p \left(e(t) + k_i \int_0^t f(t) dt \right)$

Thus, the Laplace transform of $u(t)$ is:

$U(s) = k_p \left(E(s) + k_i \frac{E(s)}{s} \right)$

Factorization by $E(s)$:

$U(s) = k_p \left(1 + \frac{k_i}{s} \right) E(s)$

The transfer function $C(s)$ of the controller is defined by $C(s) = \frac{U(s)}{E(s)}$, so:

$$C(s) = k_p \left(1 + \frac{k_i}{s} \right) \tag{14}$$

3.1.2 MPPT Algorithm based on FOPI Controller

The fractional-order PI (FOPI) controller in the time domain is governed by the following differential equation:

$$u(t) = k_p \times e(t) + k_p k_i D_t^{-\lambda} \times e(t) \tag{15}$$

Here, k_i denotes the integral gain, $e(t)$ represents the error signal, k_p is the proportional gain, and λ corresponds to the fractional order of the integral action.

Unlike the conventional PI controller, the FOPI controller employs a fractional calculus operator $D_t^{-\lambda}$. This extension provides additional flexibility in tuning, allowing for improved performance and better dynamic response. By varying the fractional order λ, it becomes possible to fine-tune the control behavior and enhance system smoothness.

Substitute the fractional integral definition:

$$u(t) = K_p \left(e(t) + \frac{K_i}{\Gamma(\lambda)} \int_0^t (t-\tau)^{\lambda-1} e(\tau) d\tau \right) \tag{16}$$

using the Laplace transform

$$U(s) = k_p \left(E(s) + k_i \frac{E(s)}{s^{\lambda}} \right) \tag{17}$$

Factor out $E(s)$

$$U(s) = k_p\left(1 + \frac{k_i}{s^{\lambda}}\right)E(s) \tag{18}$$

The transfer function $C(s)$ of the controller is defined by $C(s) = \frac{U(s)}{E(s)}$, so:

$$C(s) = k_p\left(1 + \frac{k_i}{s^{\lambda}}\right) \tag{19}$$

Figure 4 shows the controller structure, developed according to a PI^{λ} (Fractional Order PI) strategy dedicated to wind turbine speed control.

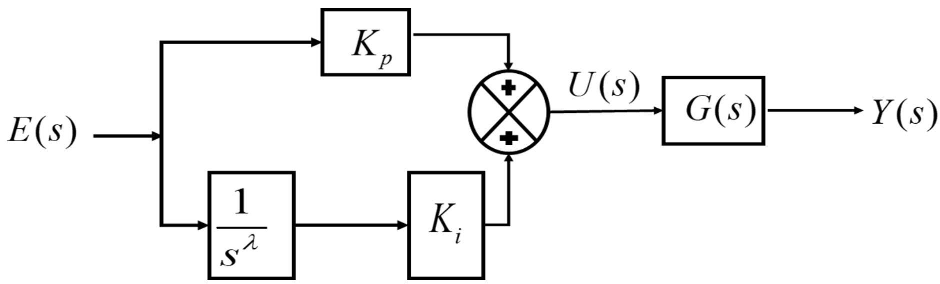

Fig.4. Block diagram of controller.

The turbine dynamics are approximated by a first-order model of the type:

$$G(s) = \frac{1}{Js + F_v} \tag{20}$$

The proposed corrector is defined by the following expression:

$$C(s) = k_p\left(1 + \frac{k_i}{s^{\lambda}}\right) \tag{21}$$

The open-loop G(s) of the wind turbine speed after application of the FOPI controller is:

$$L(s) = C(s)G(s) = k_p\left(1 + \frac{k_i}{s^{\lambda}}\right)\left(\frac{1}{Js + F_v}\right) \tag{22}$$

The Open-loop frequency response:

$$L(j\omega) = k \times k_p\left(1 + \frac{k_i}{(j\omega)^{\lambda}}\right)\left(\frac{1}{1 + T(j\omega)}\right) \tag{23}$$

With $k = \frac{1}{F_v}$, and $T = \frac{J}{F_v}$

A FOPI is mainly adjusted in three ways: optimization, placement of dominant poles, and phase margin and amplitude criteria. The phase margin and amplitude method is used in this article to design a robust controller. To ensure robustness and stability, the synthesis imposes three constraints.

(i) Phase margin condition:

$$Arg\left[L\left(j\omega_c\right)\right] = Arg\left[C\left(j\omega_c\right)G\left(j\omega_c\right)\right] = -\pi + \phi_m \quad (24)$$

(ii) (ii) Gain crossover frequency condition:

$$L\left(j\omega_c\right)dB = C\left(j\omega_c\right)G\left(j\omega_c\right)dB = 0 \quad (25)$$

(iii) Robustness to the variations of the system gain:

$$\left(\frac{d\left(Arg\left|L\left(j\omega_c\right)\right|\right)}{d\omega}\right)_{\omega=\omega_c} = 0 \quad (26)$$

$$Arg\left|L\left(\omega_c\right)\right| = -\arctan\frac{k_i\omega_c^{-\lambda}\sin\left(\lambda\frac{\pi}{2}\right)}{1+k_i\omega_c^{-\lambda}\sin\left(\lambda\frac{\pi}{2}\right)} - \arctan\left(T\omega_c\right) = -\pi + \phi_m \quad (27)$$

As mentioned in constraint (i), a relationship can be established between k_i and λ as:

$$k_i = \frac{-\tan\left[\arctan\left(T\omega_c\right)+\phi_m\right]}{\omega_c^{-\lambda}\sin\left(\lambda\frac{\pi}{2}\right)+\omega_c^{-\lambda}\cos\left(\lambda\frac{\pi}{2}\right)\times\tan\left[\arctan\left(T\omega_c\right)+\phi_m\right]} \quad (28)$$

When robustness condition (iii):

$$\left(\frac{d\left(Arg\left|L\left(j\omega_c\right)\right|\right)}{d\omega}\right)_{\omega=\omega_c} = \frac{k_i\lambda\omega_c^{\lambda-1}\sin\left(\lambda\frac{\pi}{2}\right)}{\omega_c^{2\lambda}+2k_i\omega_c^{\lambda}\cos\left(\lambda\frac{\pi}{2}\right)+k_i^2-\frac{T}{1+\left(T\omega_c\right)^2}} = 0 \quad (29)$$

Similarly, we can create another equation for based on equation (19) like this:

$$k_i = -\frac{-\sigma\pm\sqrt{\sigma^2-4C^2\omega_c^{-2\lambda}}}{2\omega_c^{-2\lambda}} \quad (30)$$

Where $C = \frac{T}{1+\left(T\omega_c\right)^2}$

And $\sigma = 2C\omega_c^{-\lambda}\cos\left(\lambda\frac{\pi}{2}\right)-\lambda\omega_c^{-\lambda-1}\sin\left(\lambda\frac{\pi}{2}\right)$

k_p can be written as mentioned in Constraint (ii):

$$k_p = \frac{\sqrt{1+\left(T\omega_c\right)^2}}{k\sqrt{\left[1+k_i\omega_c^{-\lambda}\cos\left(\lambda\frac{\pi}{2}\right)\right]^2+\left[k_i\omega_c^{-\lambda}\sin\left(\lambda\frac{\pi}{2}\right)\right]^2}} \quad (31)$$

To size the fractional PI controller, we use a MATLAB script that automatically calculates λ, K_i, and K_p from the process parameters $K=\frac{J}{F_v}$ et $K=\frac{1}{F_v}$ and the frequency specifications

(cut-off frequency ω_c and phase margin φ). The principle consists of determining λ by enforcing consistency between the expression of K_i derived from the phase condition (Eq. 28) and that deduced from the system structure (Eq. 30), retaining only the physically admissible solution ($K_i > 0$ and $K_p > 0$). The proportional gain K_p is then obtained from the modulus condition at the cut-off (Eq. 31) so that $|L(j\omega_c)| \approx 1$. The program reports the solution $= 0.2264$, $K_i = 15.6236$ and $K_p = 0.0309$). In our simulations, we selected $\omega_c = 0.002\, rad/s$ and φ=70°, which provides a setting consistent with the high inertia J of the process and meets robustness objectives.
Later, the proposed PI^{λ} controller can be shown as shown below:

$$C(s) = 0.0309\left(1 + \frac{15.6236}{s^{0.2264}}\right) \tag{32}$$

The Bode diagram in Figure 5 confirms that the system is stable and robust.

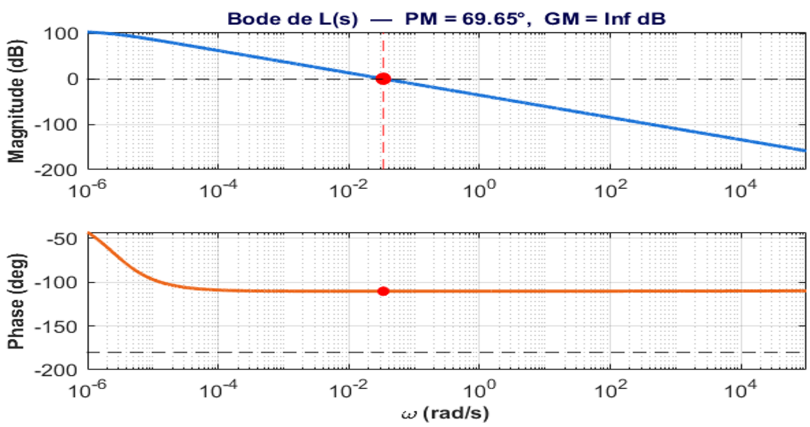

Fig.5. Bode plot of the open-loop system L(s).

4 Simulation-based outcomes

The energy conversion system, comprising a 1.5 MW wind turbine, was modeled and simulated in MATLAB/Simulink to evaluate the performance of the proposed MPPT control strategy. The system parameters relating to the wind turbine and the double-fed asynchronous generator are presented in Tables 1.
The results of the suggested methods are analysed using only a real wind case, based on measured fluctuations in wind speed in the town of Dakhla, Morocco. The evaluation results confirm excellent tracking accuracy, fast response times and high precision.

The illustration in Fig 6 displays an actual wind pattern modelled for 20 seconds in the Moroccan city of Dakhla. The wind speed fluctuates from 7. 8 m/s to 10. 5 m/s, starting with a slow rise, then speeding up, followed by a period of moderate to intense turbulence, and finally tapering off slightly towards the end of the timeframe. Such changes are characteristic of natural weather conditions and offer a significant context for evaluating the efficiency and reliability Maximum power tracking algorithms for wind power systems.
Figure 7 Demonstrates the behaviour of the power coefficient in relation to time for two control strategies: conventional PI and PI^{λ} . The results show that both methods quickly reach a quasi-constant value close to 0.48, indicating efficient tracking of the maximum

power point. However, the PI^{λ} controller stands out for its better dynamic response at start-up and increased stability, with a more accurate and constant value than the other techniques.

Table 1. Parameters of the wind turbine and DFIG generator.

Parameter	Value
Number of blades	3
Blade radius	35.25 m
Gearbox ratio	90
Friction coefficient	2.4×10^{-3} N·m·s/rad
Moment of inertia	1000 kg·m²
Rated power	1.5 MW
Stator rated frequency	50 Hz
Mutual inductance	13.5 mH
Stator inductance	13.7 mH
Rotor inductance	13.6 mH
Stator resistance	12 mΩ
Rotor resistance	21 mΩ
Number of pole pairs	2

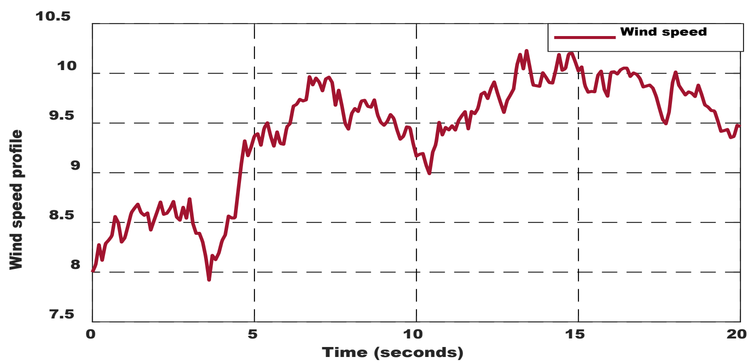

Fig.6. Wind speed of scenario.

Figure 8 illustrates the dynamic response of the tip speed ratio (TSR) related to the two controllers. It is observed that the controllers help maintain the TSR value close to the desired setpoint, though with varying degrees of accuracy.

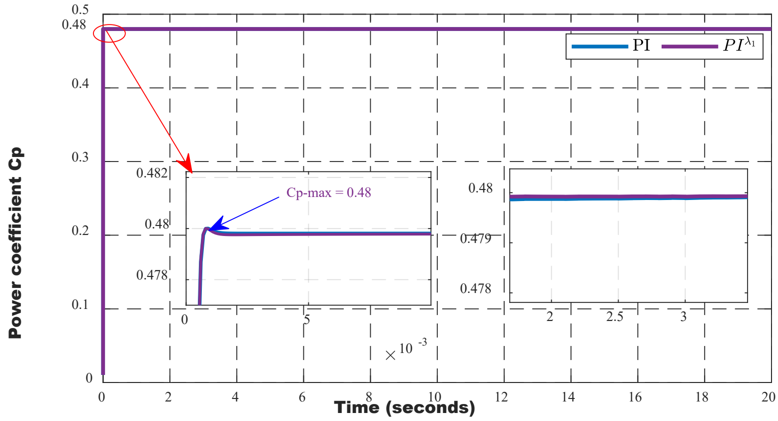

Fig.7. Wind speed of scenario.

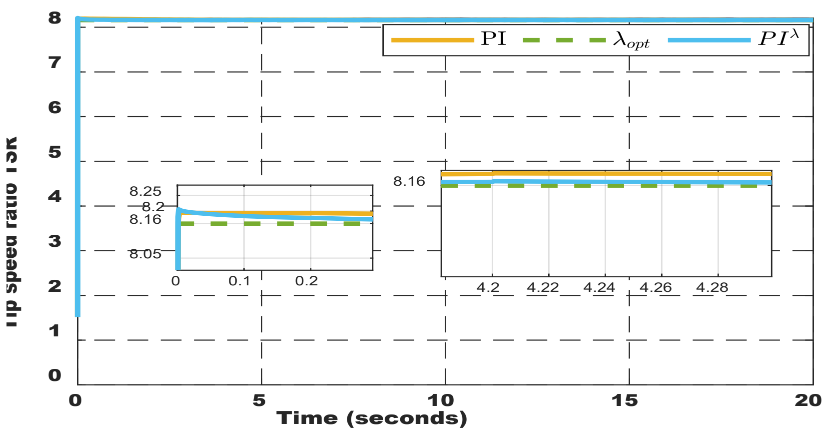

Fig.8. TSR

The controller PI^{λ}, shown in red, provides exceptionally precise control with a stable response from the outset, avoiding any fluctuations or overshoot. The enlarged boxes emphasize the regulator's ability to reach the optimal TSR value more swiftly and accurately. In contrast, the conventional PI controller shows a slight constant deviation and a slower convergence. Figure 9 shows the variation in speed error for the two types of controllers: the controller PI and the PI^{λ}. It can be seen that the traditional PI controller has a larger fluctuating error than the others. The fractional variant, on the other hand, shows a marked reduction in error, giving more reliable and accurate results, with the error remaining close to zero throughout the experiment. The enlarged part of the graph highlights the difference in performance between the two control methods over a short period.
Figure 10 shows the evolution of the angular velocity of the wind turbine over time for the two different control methods: the PI controller and the PI^{λ}. The objective is to evaluate the ability of each controller to adapt to changes in the target speed while guaranteeing dynamic stability and accuracy under different operating conditions.

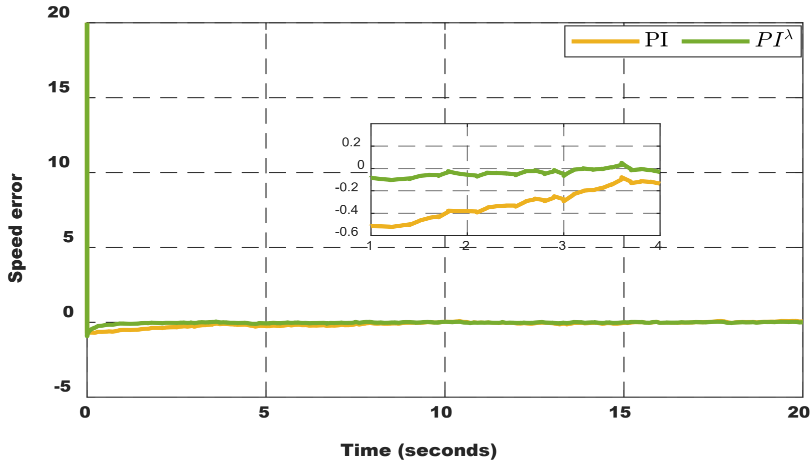

Fig.9. wind speed error

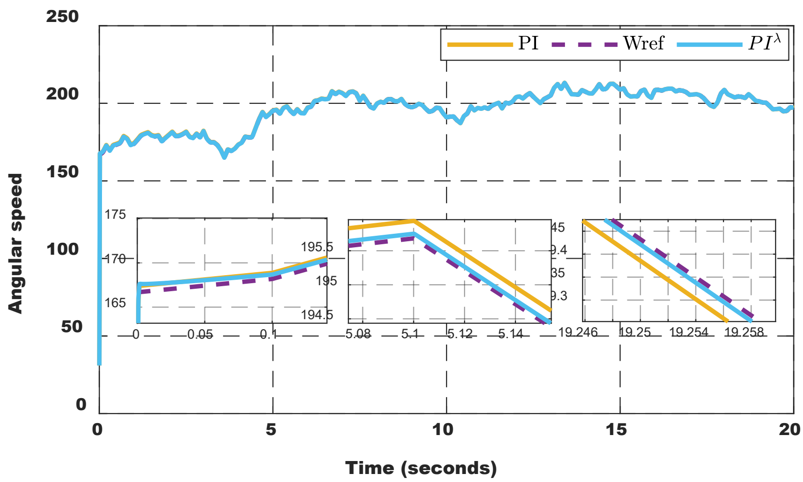

Fig.10. Rotor angular speed

In the section shown in Figure 10, the PI^{λ} controller clearly outperforms the PI controller regarding consistency and monitoring accuracy. It keeps the angular velocity of the wind turbine aligned with the desired value, while reacting well to disturbances and rapid changes. In contrast, the PI controller represented by the yellow curve shows considerable fluctuations. Table 2 above compares the performance of PI and PI^{λ} controllers according to several criteria, including static error, response time, overshoot, stability, TSR tracking accuracy, and robustness.

Table 2. Comparative wind speed study.

Controller	Steady-State Error (%)	Response Time (s)	Overshoot (%)	Stability	TSR Tracking Accuracy	Robustness
PI	0.45	0.025	0.130	Moderate	Weak	Weak
PI^{λ}	0.15	0.002	0.036	Good	Good	Good

5 Comparison of the control strategies implemented with other commonly used MPPT methods.

To place the fractional order controller in the MPPT research domain, a comparative study was conducted using common performance metrics. In our study, we carried out a comparison between our PI^{λ} method and two reference techniques, namely OTC and AFTISMC. The results clearly demonstrate the advantage of our approach. The OTC method provides average setpoint tracking, while AFTISMC performs better dynamically with a response time of 0.02488 s and satisfactory setpoint tracking. However, our method stands out with a very fast response time of 0.002 s and a low static error of 0.015%. What's more, it guarantees excellent setpoint tracking and minimized steady-state error, achieving near-zero static error and fast response time, confirming its effectiveness for wind MPPT systems. Table 3 illustrates the advantage of the proposed controller by comparing its performance to the reference values established by previous work.

Table 3. Comparison between the proposed dual fractional controller and existing work

MPPT Technique	Response Time (s)	Static Error (%)	TSR Tracking Accuracy
OTC [15]	0.02488	- - -	Good
AFTISMC [16]	- - -	0.0751	Good
Backstepping [17]	0.005	1.1	Good
Proposed	0.002	0.15	Excellent

6 Conclusion

This paper presents a robust and adaptable MPPT control method based on a PI^{λ} controller for wind energy conversion systems. Unlike conventional integer-order PI methods, the highlighted controller takes advantage of the additional degrees of freedom offered by fractional computation to improve dynamic response as well as robustness under changing wind conditions. Through exhaustive simulations, the PI^{λ} controller demonstrated faster convergence to the optimum power point, reduced steady-state error and improved adaptability, while keeping implementation simple. Its tunability enables optimal adaptation to the non-linear dynamics of wind turbines, which is crucial for maintaining optimum performance under variable wind conditions. This research enriches the growing field of studies concerning fractional control applied to renewable energy systems, and opens up interesting possibilities for real-time implementation. Future research will focus on real-time experimental validation on a dSPACE board, and the study of synergies with intelligent metaheuristic algorithms to automate parameter tuning and further improve energy harvesting efficiency.

References

1. M. Stiebler, *Wind Energy Systems for Electric Power Generation* (Springer Science & Business Media, 2008).
2. M. E. Zaman, M. A. Kayum, M. K. H. Chowdhury, and T. Barai, (2025).

3. A. Dadone and L. Dambrosio, Energy Conversion and Management **44**, 135 (2003).
4. S. Müller, M. Deicke, and R. W. De Doncker, IEEE Industry Applications Magazine **8**, 26 (2002).
5. C. Balasundar, S. Sudharshanan, and R. Elakkiyavendan, Int. J. Res. Appl. Sci. Eng. Technol **3**, (2015).
6. H. Guo, T. Qiu, and J. Jiang, J. Shanghai Jiaotong Univ. (Sci.) **17**, 209 (2012).
7. I. Jahmeerbacus and C. Bhurtun, Jahmeerbacus I., Bhurtun C.: Energize 41 (2008).
8. S. A. Rizzo and G. Scelba, Applied Energy **145**, 124 (2015).
9. R. Cárdenas and R. Pena, IEEE Transactions on Energy Conversion **19**, 196 (2004).
10. E. Koutroulis and K. Kalaitzakis, IEEE Transactions on Industrial Electronics **53**, 486 (2006).
11. S. Sabzevari, A. Karimpour, M. Monfared, and M. B. Naghibi Sistani, Journal of Renewable and Sustainable Energy **9**, (2017).
12. M. Es-Salmi, M. Taoussi, A. El Ouadiki, and A. Derouich, in *2024 3rd International Conference on Embedded Systems and Artificial Intelligence (ESAI)* (IEEE, 2024), pp. 1–8.
13. M. Taoussi, M. Karim, B. Bossoufi, D. Hammoumi, A. Lagrioui, and A. Derouich, IJAAC **10**, 12 (2016).
14. F. M. Lamine, S. Fatma, and B. Nadia, in *2019 1st International Conference on Sustainable Renewable Energy Systems and Applications (ICSRESA)* (IEEE, 2019), pp. 1–6.
15. M. Nasiri, J. Milimonfared, and S. H. Fathi, Energy Conversion and Management **86**, 892 (2014).
16. Q. Chen, L. Wang, Y. Sun, S. Xie, and R. Wang, IET Renewable Power Gen **18**, 4265 (2024).
17. M. Nadour, A. Essadki, and T. Nasser, International Journal of Renewable Energy Research **7**, 1307 (2017).